Physics Letters B 761 (2016) 247–252

Contents lists available at ScienceDirect

Physics Letters B

www.elsevier.com/locate/physletb

Constraints on the α + nucleus optical-model potential via α-induced reaction studies on ^{108}Cd

P. Scholz [a,*], F. Heim [a], J. Mayer [a], C. Münker [b], L. Netterdon [a], F. Wombacher [b], A. Zilges [a]

[a] Institute for Nuclear Physics, University of Cologne, Zülpicher Straße 77, D-50937 Cologne, Germany
[b] Joint Cologne-Bonn isotope facility at Steinmann Institut, University of Bonn, Poppelsdorfer Schloß, D-53115 Bonn, Germany

ARTICLE INFO

Article history:
Received 10 February 2016
Received in revised form 1 July 2016
Accepted 18 August 2016
Available online 24 August 2016
Editor: V. Metag

Keywords:
γ-Ray spectroscopy
Nuclear astrophysics
Cross-sections measurements
α + nucleus optical-model potential
In-beam technique
Activation method

ABSTRACT

A big part in understanding the nucleosynthesis of heavy nuclei is a proper description of the effective interaction between an α-particle and a target nucleus. Information about the so-called α + nucleus optical-model potential is achieved by precise cross-section measurements at sub-Coulomb energies aiming to constrain the theoretical models for the nuclear physics input-parameters. The cross sections of the ^{108}Cd(α,γ) and ^{108}Cd(α,n) reaction have been measured for the first time close to the astrophysically relevant energy region via the in-beam method at the high-efficiency γ-ray spectrometer HORUS and via the activation technique at the Cologne Clover Counting Setup at the Institute for Nuclear Physics in Cologne, Germany. Comparisons between experimental results and theoretical predictions calculated in the scope of the Hauser–Feshbach statistical model confirm the need for a exponentially decreasing imaginary part of the potential. Moreover, it is shown that the results presented here together with already published data indicate that a systematic investigation of the real part of the potential could help to further improve the understanding of reactions involving α-particles.

1. Introduction

The α + nucleus optical-model potential (α-OMP), thus, the effective potential between an α-particle and a target nucleus, is an important ingredient in understanding the nucleosynthesis of heavy elements. Responsible for the strength of α-channels in direct non-resonant nuclear reactions, it's characteristics determines the probability of reactions involving α-particles and therefore the reaction flux in many different nucleosynthesis processes, *e.g.* in the α-rich freeze-out [1,2], neutrino driven winds [3], and in the γ-process in Type Ia and Type II SNe [4–6], and in the αp-process at the beginning of the rapid proton-capture process [7]. This means that the construction of a reliable and global α-OMP will put reaction networks of a various set of nucleosynthesis processes on a much firmer basis.

During the last years, enormous effort was put in measuring α-induced reaction cross-section on target nuclei of a wide mass range in order to constrain or exclude different theoretical models for the α-OMP [8–20]. It was shown that in many cases calculations using the most widely adopted α-OMP by McFadden and Satchler [21] overestimate the experimental cross-section values at low interaction energies. Even in cases in which uncertainties from other nuclear physics input-parameters like the γ-ray strength-function or the nuclear level density could be neglected, it was observed that the lower the center-of-mass energy, the higher the discrepancy between the experimental and calculated values (see, *e.g.*, [17] and references therein).

Recently, it has been claimed that the exponentially decreasing absorption of an α-particle at sub-Coloumb energies can be due to an inadequate treatment of Coulomb excitation (Coulex) as a direct reaction channel in the Hauser–Feshbach statistical model [22]. By renormalizing the compound formation cross section using the Coulex cross section for each partial wave of the incoming α flux, the Hauser–Feshbach cross sections were reduced as much as it was needed for a proper description of the experimental data for the ^{141}Pr$(\alpha,n)^{144}$Pm [10] and ^{169}Tm$(\alpha,n)^{172}$Lu reaction [23] using the α-OMP of McFadden and Satchler. Although these results are very promising, the cross-section measurement of the ^{64}Zn$(p,\alpha)^{61}$Cu reaction [24] has shown that with the α-particle in the exit channel the α-OMP seems not to be correct.

However, a fairly good description of the experimental values of the ^{144}Sm$(\alpha,\gamma)^{148}$Gd reaction was found by modifying the imaginary part of the α-OMP with an energy-dependent

* Corresponding author.
E-mail address: pscholz@ikp.uni-koeln.de (P. Scholz).

http://dx.doi.org/10.1016/j.physletb.2016.08.040

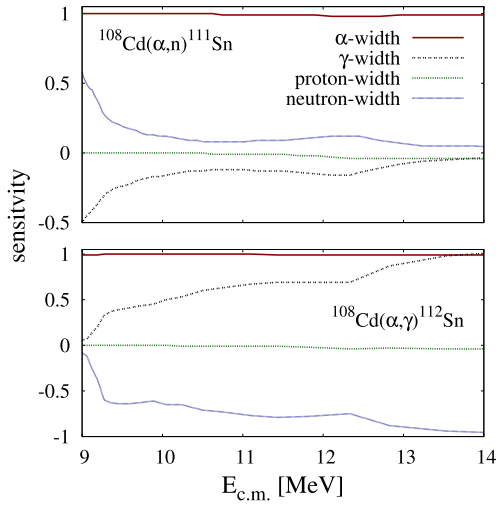

Fig. 1. (Color online.) Sensitivities for the (α, n) and (α, γ) reaction on the p nucleus ^{108}Cd to changes in the α, γ, neutron, and proton widths [27].

Fermi-type function [25]. This idea influenced the development of a semi-microscopic α-OMP by P. Demetriou et al. in 2002 [26]. They presented three different versions of an α-OMP, all of them with an energy-dependent Fermi-type imaginary part, which were very useful in describing the – at that time – rare experimental database of (α, γ)-reaction cross-sections at sub-Coulomb energies. However, recent cross-section measurements of α-induced reactions on heavy nuclei have revealed problems with the α-OMP of Demetriou et al., *e.g.* ^{168}Yb$(\alpha, \gamma)^{172}$Hf, ^{168}Yb$(\alpha, n)^{171}$Hf [16], ^{187}Re$(\alpha, n)^{190}$Ir [17], ^{166}Er$(\alpha, n)^{169}$Yb and ^{166}Er$(\alpha, n)^{169}$Yb [18], and ^{112}Sn$(\alpha, \gamma)^{116}$Te [19]. In these cases modifications of the α-OMP of either McFadden & Satchler or P. Demetriou et al. were presented to reproduce the experimental values.

The experiments presented here were aimed at testing the α-OMPs and also their recent modifications on the p nucleus ^{108}Cd. In Fig. 1 the sensitivities of the ^{108}Cd$(\alpha, \gamma)^{112}$Sn and ^{108}Cd$(\alpha, n)^{111}$Sn reaction cross-section to changes in single decay widths is shown as calculated in Ref. [27]. In an energy range between 9.5 MeV and 14 MeV the ^{108}Cd$(\alpha, \gamma)^{112}$Sn reaction cross-section is very sensitive to changes in either the α, or the neutron and γ widths. Since the ^{108}Cd$(\alpha, n)^{111}$Sn reaction measured cross-section values for this reaction can be expected to be almost only sensitive to the α-OMP, an simultaneous measurement of the (α, n) reaction cross-section reduces the uncertainty in the description of this input-parameter. In this work, cross-section values for both reactions were measured, the ^{108}Cd$(\alpha, \gamma)^{112}$Sn via the in-beam method with high-purity germanium detectors (HPGe) at the high efficiency γ-ray spectrometer HORUS at the University of Cologne (see Sec. 3) and the ^{108}Cd$(\alpha, n)^{111}$Sn via the activation method at the Cologne Clover Counting Setup (see Sec. 4). An comparison of the experimental results and statistical model calculations is given in Sec. 5.

2. Using mass spectrometry for the characterization of the target properties

For the production of the targets, Cd metal with an enriched ^{108}Cd isotope abundance of 70.6% was used. After dissolving the Cd metal in 10% sulfuric acid it was secluded on a 48 $\frac{\mu g}{cm^2}$ thick gold foil via electrolysis. The gold foil with the cadmium layer on top was then used to produce two targets. At first, we attempted to measure the thickness of the targets by means of Rutherford-Backscattering Spectrometry (RBS) at the Ruhruniversität Bochum, Germany. However, after a short time the Cd layer started to alloy with the gold backing. The expected layer structure of the cadmium-gold targets started already to smear, hampering a reliable determination of the layer thicknesses. A second RBS measurement after the experimental campaign revealed an even worse situation. Apparently, the irradiation has supported the alloy process. Eventually, the thickness of the targets was recalculated from the mass of Cd in the targets. The mass of Cd was determined by isotope dilution mass spectrometry. To this end, both targets were completely dissolved in *aqua regia* and then diluted with 0.14 M HNO_3. Three aliquots for each target were then mixed in different proportions with a commercial Cd calibration solution (Merck KgaA) with a natural Cd isotope composition. Cadmium isotope ratios of these mixtures, the pure Cd standard, and the enriched ^{108}Cd from the targets were then performed using the Neptune multiple collector inductively coupled plasma mass spectrometer [28] at the Steinmann Institute in Bonn, Germany. The instrumental setup was similar to that reported in Ref. [29]. Using two sets of measurements, ion beams of ^{105}Pd, ^{106}Cd, ^{108}Cd, ^{110}Cd, ^{112}Cd, ^{113}Cd, ^{115}In, ^{114}Cd, ^{116}Cd, and ^{117}Sn relative to the ^{111}Cd ion beam were integrated for about 3 minutes on Faraday collectors. Background analysis were carried out before each sample analysis, after rinsing the sample introduction system for four minutes with 0.14 M HNO_3. Background subtraction and Pd, In and Sn interference corrections were carried out but had negligible effects on the results. The instrumental mass discrimination was corrected using the exponential mass fractionation law of Ref. [30], ^{114}Cd/^{110}Cd = 2.24453 [31] and repeated analysis of the Merck calibration solution at the beginning and end of the measurement session. Results from three isotope dilution analysis for each target agreed within better than 0.04%. Conservatively, the combined uncertainty of the mass of the enriched Cd on the targets was estimated to 1%. In order to calculate an areal particle density as needed for the cross-section measurements, the area of the cadmium layer was determined via photometric analysis of target photographs taken shortly after their production. However, the determination of the cadmium layer area is not as accurate and an uncertainty of 15% was taken into account. The details of the mass measurement as well as the obtained thicknesses are listed in Table 1 of the supplementary material. The energy-loss ΔE of the impinging α particles in the target material and therefore the correction for the beam energy was achieved via a series of simulations using SRIM/TRIM (v. 2013) [32]. Hence, the effective α-particle energy E_α was calculated via

$$E_\alpha = E_0 - \frac{\Delta E}{2} \tag{1}$$

where E_0 is the beam energy and ΔE was found to be 27 keV.

3. In-beam Measurement of the ^{108}Cd$(\alpha, \gamma)^{112}$Sn reaction cross section

First, the experiment was focused on the measurement of cross-section values for the ^{108}Cd$(\alpha, \gamma)^{112}$Sn reaction via the in-beam technique at the high-efficiency γ-ray spectrometer HORUS [33] at four α-particle energies between 12 MeV and 13.5 MeV. The α-particle beam was delivered by the 10 MV FN-Tandem accelerator of the Institute for Nuclear Physics at the University of Cologne to a target chamber specifically designed for Nuclear Astrophysics experiments [33].

Fourteen high-purity germanium detectors (HPGe) of the HORUS spectrometer, partly equipped with BGO shields for an active Compton suppression, are placed under five different angles relative to the beam axis. Hence it is possible to measure angular distributions of the γ-ray transitions to the ground state of ^{112}Sn

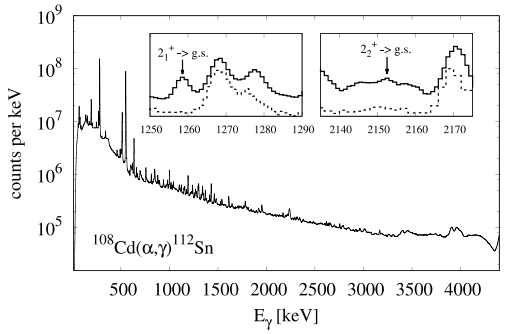

Fig. 2. In-beam spectrum summed for all detectors perpendicular to the beam axis at an α-particle energy of 13.5 MeV (solid line). The insets are showing the two $2^+ \rightarrow 0^+$ ground-state transitions which were used for the calculation of the (α, γ) cross section. Most of the peaks visible in the spectrum are stemming from (α, n) reactions on copper and zinc isotopes, which were the main contaminant in the target material, as well as transitions from gold, and the (α, n) reaction product ^{111}Sn. In addition, a spectrum taken for the measurement of the backing material is shown (dashed line) and scaled in favor of a better readability.

which are needed to determine the number of produced compound nuclei and, therefore, the total cross-section values for the ^{108}Cd(α, γ) reaction. For this purpose, the intensities normalized to the full-energy peak efficiency and the relative dead time of all detectors for one γ-ray transition γ_i to the ground state as a function of the angle relative to the beam axis $W^i(\theta)$ are fitted via a series of Legendre polynomials:

$$W^i(\theta) = A_0^i \left(1 + \sum_{k=2,4} \alpha_k P_k(\cos\theta) \right). \quad (2)$$

The cross-section value for a certain energy can then be calculated from the absolute coefficients of the respective angular distributions A_0^i:

$$\sigma = \frac{\sum_{i=1}^{N} A_0^i}{m_t N_\alpha}, \quad (3)$$

where N is the total number of considered γ-ray transitions, m_t the areal density of target nuclei, and N_α the number of impinged α particles. The experimental in-beam method at the HORUS spectrometer is described in detail in Ref. [33]. Despite irradiating the targets 2 to 4 days per energy with an α-particle beam current between 100 nA and 250 nA not all ground-state transitions in ^{112}Sn became visible in the γ-ray spectra, see Fig. 2. Only for the first two $2^+ \rightarrow 0^+$ γ-ray transitions to the ground-state in ^{112}Sn, *i.e.*, 1257.05 keV and 2151 keV [34], it was possible to measure angular distributions. Contributions from γ-transitions of other sources were investigated via the measurement of $\gamma\gamma$ coincidences and the analysis of spectra measured while irradiating the gold backing at each energy. However, it was possible to determine upper limits for the contributions from the other ground-state transitions to the total reaction cross-section. The contributions of each of all the other ground-state transitions was found to be less than 1%. For a more detailed discussion of other ground-state transitions we refer to the supplementary material. The obtained cross-section values for the ^{108}Cd$(\alpha, \gamma)^{112}$Sn are given in Table 2 of the supplementary material and are shown in Fig. 3.

4. Activation method applied on the ^{108}Cd$(\alpha, n)^{111}$Sn reaction

The second part of the experiment was focused on the measurement of the ^{108}Cd$(\alpha, n)^{111}$Sn cross-section values. For α-particle energies between 12 MeV and 13.5 MeV the cross-section values were measured simultaneously to the in-beam measurement

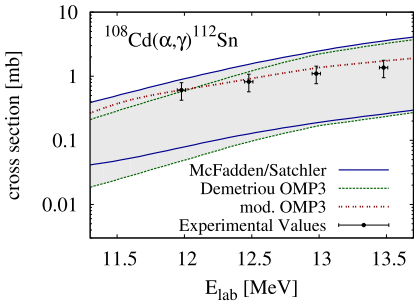

Fig. 3. (Color online.) Measured cross-section values of the ^{108}Cd$(\alpha, \gamma)^{112}$Sn reaction. Additionally, cross-section values calculated using the statistical model code TALYS (v1.6) are shown, in blue calculated based on the α-OMP of Ref. [21] (McFadden/Satchler) and in green based on the α-OMP of Ref. [26] (Demtriou OMP3), respectively. The gray shaded areas indicate the region of calculated values obtained by variation of the input-parameter models for the nuclear-level density and the γ-ray strength function. Upper and lower limits are shown as solid lines. The dashed red line corresponds to calculations based on the modification of the α-OMP of Demetriou et al. See text for details.

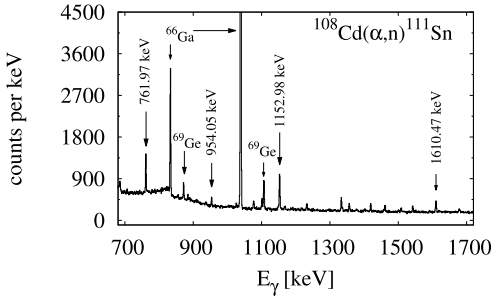

Fig. 4. Spectrum measured after the activation of ^{108}Cd with an 12.5 MeV α-particle beam. The spectrum includes measured events for 6.5 h of counting time. The γ-ray transitions used for the analysis are labeled with their specific γ-ray energies. Also visible with a rather large intensity are γ-ray transitions following the decay of the ^{63}Cu(α, n) and ^{66}Zn(α, n) reaction products ^{66}Ga and ^{69}Ge, respectively.

applying the activation method using the Cologne Clover Counting Setup [10,16,17] during the first part of the experiment. Additionally, the measurements were later extended down to α-particle energies of 10.2 MeV, while the 12.0 MeV measurement was repeated in order to exclude systematic errors. For 13.5 MeV and 13.0 MeV the intensities in the γ-ray spectra of each clover detector were sufficient to determine individual cross-section values. Below these energies, the obtained spectra for the single crystals of both clover detectors were summed up. An activation at 13.0 MeV was performed twice during the first part of the experimental campaign.

After the irradiation of ^{108}Cd with an α-particle beam, the target was transported within less than 10 min to the Cologne Clover Counting Setup in order to measure the subsequent γ-rays following the β^+-decay of ^{111}Sn with an half-life of 35.4 min [34]. The Cologne Clover Counting setup consists of two HPGe clover detectors in a very close face-to-face geometry [10,16,17]. Fig. 4 shows a typical spectrum for the activation measurement at 12.5 MeV which was measured for approx. 6.5 h

Once the number of events for a γ-ray transition N_γ with the γ-ray intensity I_γ in the γ-ray spectra (see Fig. 4) was determined, the specific cross-section values can be calculated:

$$\sigma = \frac{\lambda N_\gamma \cdot e^{\lambda t_W}}{m_t \tau I_\gamma \epsilon_\gamma \left(1 - e^{-\lambda t_C}\right)} \times f_{ac}. \quad (4)$$

Here, t_W denotes the time between the end of the irradiation and the beginning of the counting and t_C the time of measurement with the Cologne Clover Counting Setup, respectively. The

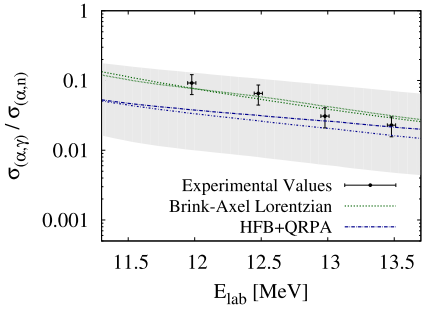

Fig. 5. (Color online.) The ratios between the (α,γ) and the (α,n) cross-section values compared to TALYS calculations based on different models for the γ-ray strength function and the nuclear level density. Only the calculated values for the γ-ray strength function models with the best reproduction are plotted. The overall range of obtained values by variation over all available models for these input-parameters is indicated by a gray shaded area. See text for details.

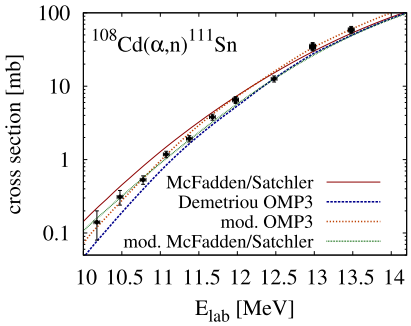

Fig. 6. (Color online.) The measured (α,n) cross-section values compared to statistical model calculations using different models for the α-OMP. See text for details.

factor f_{ac} corrects for decaying nuclei during the irradiation and the non-constant particle-flux [17].

The efficiencies of the clover detectors as well as the summing corrections factors were obtained as in Ref. [17]. Information about detector efficiencies and the obtained cross-section values for the ^{108}Cd(α,n) reaction are listed in Table 3 and 4 of the supplementary material.

5. Discussion and implications

The cross-section values measured for both α-induced reactions on the p nucleus ^{108}Cd were compared to predictions of statistical model calculations. All calculations were performed using the TALYS code [35] in version 1.6. As mentioned in Sec. 1, it is not possible to constrain any model for the α-OMP by comparing the (α,γ) cross-section values to statistical model calculations due to its sensitivity on too many different nuclear physics input-parameters (see Fig. 1). However, the ratio between (α,γ) and (α,n) cross-section values can be used to remove the sensitivity to the adopted model for the α-OMP, since

$$\frac{\sigma_{(\alpha,\gamma)}}{\sigma_{(\alpha,n)}} \propto \frac{T^i_\alpha T^i_\gamma}{\sum_j T^i_j} \times \frac{\sum_j T^i_j}{T^i_\alpha T^i_n} = \frac{T^i_\gamma}{T^i_n} \tag{5}$$

from the Hauser–Feshbach calculations is independent of the α transmission coefficient for sufficiently high energies. Here, T^i_j stands for the different transmission coefficients forming or decaying from the i-th compound state. The ratio was calculated for the cross-section values at energies where they were measured for both reactions, see Fig. 5. These ratios were compared to statistical model calculations by varying the models for the γ-ray strength functions and the nuclear-level density included in the TALYS code. It was found that the ratio of the cross-section values is much more sensitive to the input for the γ-ray strength function than on the different models for the nuclear level density. Hence, in Fig. 5 only the values calculated for the two best-fitting γ-ray strength function models are presented. The range of calculated values which can be achieved by variation over the whole set of available models for these two nuclear physics input-parameter in TALYS is indicated by a gray shaded area. The best reproduction of the measured ratios was obtained by the combination of the Brink-Axel Lorenzian model for the γ-ray strength function an the Back-shifted Fermi gas model for the nuclear-level density. Please note that this does not imply directly that these models are the best in describing the nuclear level density or the γ-ray strength functions in the compound nucleus ^{112}Sn but have only been found in combination to reproduce the ratio of the γ- and neutron width at best. In Fig. 6, the cross-section values measured for the (α,n) reaction are shown. Using the best models for the nuclear-level density and the γ-ray strength function, statistical model calculations were performed based on different inputs for the α-OMP. For the highest energies, the best description is given by using the α-OMP of McFadden/Satchler, although the measured values seem to be a bit underestimated. However, the same problem as in other recent measurements becomes visible towards lower interaction-energies – the deviation between the predictions of the McFadden/Satchler potential and the measured values gets larger. The results for the dispersive potential of Demetriou et al. ("Demetriou OMP3" in Fig. 6) are giving the best reproduction of the trend in energy but seem to be systematically too low. As mentioned in Ref. [26], the real part of the potential is obtained in the framework of the double-folding (DF) model of Kobos et al. [36]. Furthermore, it is stated that this procedure is only describing the shape of the potential directly, but its strength has to be adjusted in order to reproduce the experimental data according to

$$V(r) = \lambda \cdot V_{DF}(r) \tag{6}$$

This adjustment was recently done in the case of ^{112}Sn, resulting in a very good agreement between the experimental and the calculated values [19]. Moreover, calculations have already shown that the same adjustments improve also the description of cross-section data for ^{112}Sn$(\alpha,p)^{115}$Sb [37], for ^{106}Cd(α,γ) and ^{106}Cd(α,n) [38] as well as for (α,n) reactions on ^{115}Sn and ^{116}Sn [39]. Using the same normalization factor as in Ref. [19], *i.e.*, $\lambda = 1.16$, the modified OMP3 gives the best description for the ^{108}Cd(α,n) cross-section values. For the (α,γ) reaction the same statistical model calculation (red dashed line in Fig. 3) reproduces the experimental values fairly well, although at higher energies the predictions seem to overestimate the measured data slightly. This can be of course due to deviations from the real ratio of γ and neutron width at higher energies, see Fig. 5. Using the modifications on the McFadden/Satchler potential as reported, *e.g.*, in Refs. [10,16–18], helps to reproduce the trend in energies by varying the steepness parameter for the energy-dependence in the imaginary part of the potential. As an example, calculations using a steepness parameter of $a = 4$ MeV are shown as "mod. McFadden/Satchler" in Fig. 6. However, the cross section values at higher energies are still too low and an adjustment of either the depth of the real-part or the imaginary-part of the potential has to be done in order to properly describe the experimental values. Such modifications were already considered for different mass regions in Ref. [21] but were only applied for a few cases.

Nevertheless, that such modification might be inevitable can also be, for instance, shown for the (α,n) cross-section measurement on the isotope ^{165}Ho as reported in Ref. [18]. For this reaction, the results for the OMP3 of Demetriou et al. have also been found to underestimate systematically the cross-section values. As

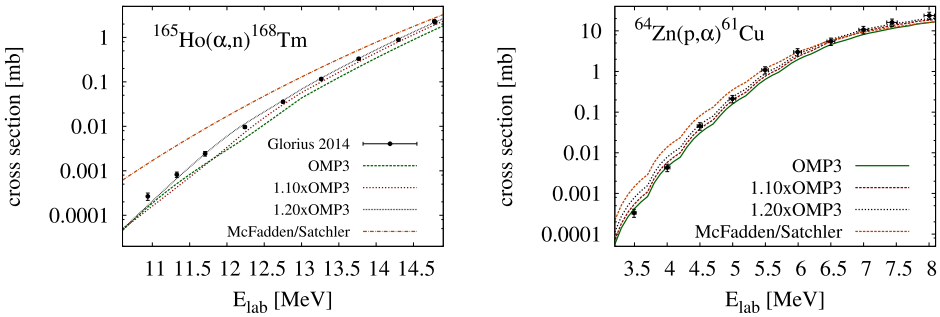

Fig. 7. (Color online.) The (α, n) cross-section results for ^{165}Ho of Ref. [18] (left) and results of the ^{64}Zn(p, α) cross-section measurement of Ref. [24] (right) compared to statistical model calculations using different values for λ for the α-OMP of Demetriou et al. ("OMP3"). By only changing the renormalization factor of the real-part of the α-OMP a fairly good description of the experimental values can be found.

shown in Fig. 7 (left), performing statistical model calculations by using different normalization factors λ between 1.0 and 1.2, a proper reproduction of the experimental values can be achieved. Hence, adjustments of the real part of the potential by Demetriou et al. might also help in describing cross-section values of other reactions. In fact, calculations for other recently published (α, n) reaction cross sections have shown comparable results. Figures 1 to 7 of the supplementary material show results of these calculations for the reactions ^{107}Ag(α, n) [40], ^{130}Ba(α, n) [15], ^{141}Pr(α, n) [10], ^{162}Er(α, n) [41], ^{166}Er(α, n) [18], ^{168}Yb(α, n) [16], ^{187}Re(α, n) [17], and ^{120}Te(α, n) [42]. Almost all of these measured reaction values can be fairly well described using the α-OMP of Demetriou *et* al. by only increasing the λ-factor of Eq. (6). Note, that all of these reactions are almost exclusively sensitive to the α width at higher energies but also quite sensitive to the γ and neutron width at lower energies. In addition, the same statistical model calculations were performed for the results of the ^{64}Zn$(p, \alpha)^{61}$Cu reaction cross-section measurement [24]. The left hand side of Fig. 7 shows, that at higher energies the measured values are also in a good agreement with the results by the modified OMP3 model, although the overall energy trend towards lower energies might be steeper than predicted by this model.

6. Conclusion

The new cross-section measurements of the α-induced reactions on the p nucleus ^{108}Cd and their comparison to statistical model calculations have shown that they are best described using the dispersive α-OMP of Ref. [26] with a slightly adjusted depth of the real-part of the potential. The same procedure was already successfully applied for the recently published ^{112}Sn(α, γ) cross-section measurement [19]. Further calculations using the same modifications for a set of (α, n) reactions revealed that this α-OMP is practically able to describe the experimental data in a mass range of $107 \leq A \leq 187$ in most cases better than the α-OMP of McFadden/Satchler [21]. The results support further investigations on the real-part of the potential through, e.g., precise α-scattering experiments at rather low energies. In order to test the α-OMP on (α, γ) data at low energies, additional information about, for instance, the γ-ray strength function are of utmost importance.

Acknowledgements

The authors thank A. Dewald and the accelerator staff at the Institute for Nuclear Physics in Cologne for providing excellent beams. Moreover, we gratefully acknowledge K. O. Zell and A. Blazhev for the target production, H.-W. Becker and D. Rogalla of the Ruhr-Universität Bochum for the assistance during RBS measurements. This project was supported by the Deutsche Forschungsgemeinschaft (INST 216/544-1, ZI 510/8-1) and the ULDETIS project within the UoC Excellence Initiative institutional strategy. PS and JM are supported by the Bonn-Cologne Graduate School of Physics and Astronomy.

Appendix A. Supplementary material

Supplementary material related to this article can be found online at http://dx.doi.org/10.1016/j.physletb.2016.08.040.

References

[1] S.E. Woosley, R.D. Hoffman, Astrophys. J. 395 (1992) 202.
[2] J. Witti, H.-Th. Janka, K. Takahashi, Astron. Astrophys. 286 (1994) 841.
[3] A. Arcones, J. Bliss, J. Phys. G, Nucl. Part. Phys. 41 (2014) 04400.
[4] S.E. Woosley, W.M. Howard, Astrophys. J. Suppl. Ser. 36 (1978) 285.
[5] M. Rayet, M. Arnould, M. Hashimoto, N. Prantzos, K. Nomoto, Astron. Astrophys. 298 (1995) 517.
[6] C. Travaglio, R. Gallino, T. Rauscher, N. Dauphas, F.K. Röpke, W. Hillebrandt, Astrophys. J. 795 (2014) 795.
[7] M. Wiescher, Europhys. Lett. 109 (2015) 62001.
[8] C. Yalçin, et al., Phys. Rev. C 79 (2009) 065801.
[9] Gy. Gyürky, et al., J. Phys. G 37 (2010) 115201.
[10] A. Sauerwein, H.-W. Becker, H. Dombrowski, M. Elvers, J. Endres, U. Giesen, J. Hasper, A. Hennig, L. Netterdon, T. Rauscher, D. Rogalla, K.O. Zell, A. Zilges, Phys. Rev. C 84 (2011) 045808.
[11] G.G. Kiss, et al., Phys. Lett. B 695 (2011) 419.
[12] G.G. Kiss, et al., Nucl. Phys. A 867 (2011).
[13] Gy. Gyürky, et al., Phys. Rev. C 86 (2012) 041601(R).
[14] G.G. Kiss, et al., Phys. Rev. C 86 (2012) 03580.
[15] Z. Halász, et al., Phys. Rev. C 85 (2012) 025804.
[16] L. Netterdon, P. Demetriou, J. Endres, U. Giesen, G.G. Kiss, A. Sauerwein, T. Szücs, K.O. Zell, A. Zilges, Nucl. Phys. A 916 (2013) 149.
[17] P. Scholz, A. Endres, A. Hennig, L. Netterdon, H.-W. Becker, J. Endres, J. Mayer, U. Giesen, D. Rogalla, F. Schlüter, S.G. Pickstone, K.O. Zell, A. Zilges, Phys. Rev. C 90 (2014) 065807.
[18] J. Glorius, K. Sonnabend, J. Görres, D. Robertson, M. Knörzer, A. Kontos, T. Rauscher, R. Reifahrt, A. Sauerwein, E. Stech, W. Tan, T. Thomas, M. Wiescher, Phys. Rev. C 89 (2014) 065808.
[19] L. Netterdon, J. Mayer, P. Scholz, A. Zilges, Phys. Rev. C 91 (2015) 035801.
[20] A. Simon, M. Beard, A. Spyrou, S.J. Quinn, B. Bucher, M. Couder, P.A. DeYoung, A.C. Dombos, J. Görres, A. Kontos, et al., Phys. Rev. C 92 (2015) 025806.
[21] L. McFadden, G.R. Satchler, Nucl. Phys. 84 (1966) 177.
[22] T. Rauscher, Phys. Rev. Lett. 111 (2013) 061104.
[23] T. Rauscher, G.G. Kiss, T. Szücs, Z. Fülöp, C. Fröhlich, G. Gyürky, Z. Halász, Z. Kertész, E. Somorjai, Phys. Rev. C 86 (2012) 015804.
[24] Gy. Gyürky, Zs. Fülöp, Z. Halász, G.G. Kiss, T. Szücs, Phys. Rev. C 90 (2014) 052801(R).
[25] E. Somorjai, Zs. Fülöp, Á.Z. Kiss, C.E. Rolfs, H.P. Trautvetter, U. Greife, M. Junker, S. Goriely, M. Arnould, M. Rayet, T. Rauscher, H. Oberhummer, Astron. Astrophys. 333 (1998) 1112–1116.
[26] P. Demetriou, C. Grama, S. Goriely, Nucl. Phys. A 707 (2002) 253.
[27] T. Rauscher, Astrophys. J. Suppl. Ser. 201 (26) (2012).

[28] M.E. Wieser, J.B. Schwieters, The development of multiple collector mass spectrometry for isotope ratio measurements, Int. J. Mass Spectrom. 242 (2005) 97–115.
[29] W. Abouchami, S.J.G. Galer, T.J. Horner, M. Rehkämper, F. Wombacher, Z. Xue, M. Lambelet, et al., A common reference material for cadmium isotope studies – NIST SRM 3108, Geostand. Geoanal. Res. 37 (1) (March 2013) 5–17, http://dx.doi.org/10.1111/j.1751-908X.2012.00175.x.
[30] W.A. Russel, D.A. Papanastassiou, T.A. Tombrello, Ca isotope fractionation on the Earth and other solar system materials, Geochim. Cosmochim. Acta 42 (1978) 1075–1090.
[31] M. Berglund, M.E. Wieser, Pure Appl. Chem. 83 (2011) 397–410.
[32] J. Ziegler, J. Biersack, M. Ziegler, SRIM – The Stopping and Range of Ions in Matter, 1996.
[33] L. Netterdon, et al., Nucl. Instrum. Methods A 754 (2014) 94.
[34] E. Browne, Nucl. Data Sheets 82 (1997) 379, accessed via National Nuclear Data Center, ENSDF database, http://nndc.bnl.gov/ensdf, last access 2014/10/28.
[35] A. Koning, S. Hilaire, M. Duijvestijn, in: O. Bersillon, F. Gunsing, E. Bauge, R. Jacqmin, S. Leray (Eds.), Presented at the Proceedings of the International Conference on Nuclear Data for Science and Technology, 22–27 April 2007, Nice, France, 2007, pp. 211–214.
[36] A.M. Kobos, et al., Nucl. Phys. A 425 (1984) 205.
[37] N. Özkan, G. Efe, R.T. Güray, A. Palumbo, J. Görres, et al., Phys. Rev. C 75 (2007) 025801.
[38] Gy. Gyürky, G.G. Kiss, Z. Elekes, Zs. Fülöp, E. Somorjai, et al., Phys. Rev. C 74 (2006) 025805.
[39] D. Filipescu, V. Avrigeanu, T. Glodariu, C. Mihai, D. Bucurescu, et al., Phys. Rev. C 83 (2011) 064609.
[40] C. Yalçin, et al., Phys. Rev. C 91 (2015) 034610.
[41] G.G. Kiss, et al., Phys. Lett. B 735 (2014) 40.
[42] A. Palumbo, W.P. Tan, J. Görres, M. Wiescher, et al., Phys. Rev. C 85 (2012) 028801.